*J. Fluid Mech.* (1979), *vol.* 95, *part* 3, *pp.* 539–565
*Printed in Great Britain*



# On the interpretation of dynamic contact angles in capillaries

By FRED Y. KAFKA† AND E. B. DUSSAN V.

Department of Chemical and Biochemical Engineering,
University of Pennsylvania, Philadelphia, Pennsylvania 19174

(Received 17 February 1978)

The motion of two immiscible fluids with arbitrary viscosities flowing through a capillary with an almost flat fluid–fluid interface is investigated in the limit of small capillary and Reynolds numbers. A complete description of the dynamics of the fluids is presented. It is shown that the motion of the fluid away from the moving contact line can be completely determined in terms of *one* material parameter, and how the capillary can be viewed as a device for measuring it. The dynamic behaviour of various contact angles, measured by others, is calculated. It is shown that they all depend on the radius of the capillary; hence, they do not represent properties of only the materials of the system.

## 1. Introduction

West (1911) and Washburn (1921) were the first to successfully analyse the displacement of one immiscible fluid by another through a circular capillary. West, interested in developing a viscometer, studied the speed at which an entrapped index of liquid moves through a capillary when a fixed pressure drop is maintained between its ends. Washburn examined the unsteady rate at which a liquid penetrates a horizontal or vertical capillary in the hopes that it would lead to a better understanding of flow through porous media. Although both were interested in different problems, their methods of analysis were the same. Their two main assumptions were: (i) the liquids undergo Poiseuille flow; (ii) the pressure drop across the spherically shaped menisci is given by the same formula used under static conditions. For the simple steady flow illustrated in figure 1, these assumptions imply that the pressure drop between $z = -L_A$ in the advancing fluid and $Z = L_R$ in the receding fluid is given by

$$P(-L_A) - P(L_R) = \frac{8U}{a^2}(\mu_A L_A + \mu_R L_R) - \frac{2\gamma}{a}\cos\theta_w, \tag{1.1}$$

where $a$ is the radius of the capillary; $\mu_A$ and $\mu_R$ are the viscosities of the advancing and receding fluids, respectively; $U$ is the speed of the meniscus relative to the capillary; $\gamma$ is the surface tension of the fluid–fluid interface; and $\theta_w$ is the dynamic value of the contact angle.

Undoubtedly, there is a certain amount of error associated with the above approach; for example, end effects and the influence of the viscous forces on the shape of the meniscus have both been ignored. However, this approach has proven to be surprisingly

† Present address: E. I. Du Pont De Nemairs & Company, Experimental Station–B/304, Wilmington, DE 19898.

0022–1120/79/4290–7360 $02.00 

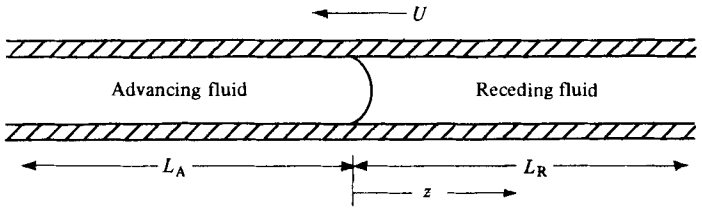


FIGURE 1. The receding fluid is being displaced by the advancing fluid. The frame of reference is at rest with respect to the contact line; consequently, the capillary is moving from right to left.

good when $Ua\rho/\mu$ and $U\mu/\gamma$ are small. By measuring the speed of entrapped mercury indices of known length and subject to known pressure drops in capillaries of various radii, West and Yarnold (1938) were able to determine the viscosity of mercury to within 7%.† Another way of assessing the accuracy of this approach is to compare the values of the contact angle which (1.1) predicts from experimentally measured values of the pressure drop, $U$, $\mu$, $a$, $L$ and $\gamma$, with that measured directly by optical means. Rose & Heins (1962), upon observing an index of oil moving through a glass capillary, found good agreement, although the scatter in their data is considerable. Blake (1968) found that the two methods always agreed to within his experimental error of $\pm 2°$ for both benzene displacing water and water displacing benzene through a glass capillary (his experiments were restricted to very small $U$, $10^{-6} \lesssim U\mu/\gamma \lesssim 10^{-3}$).

Besides its direct application to technology, for which West's approach of determining the volumetric flow rate seems to be sufficient, there remains an important scientific reason for studying the displacement of immiscible fluids through a capillary. Due to its compactness and symmetry, it is a convenient system for studying the dynamic behaviour of the contact angle. Hansen & Toong (1971), based on an interesting though *ad hoc* hydrodynamic analysis, were the first to point out that the contact angle everyone measures in the capillary is probably not its actual value due to the fact that viscous forces may severely deform the shape of the fluid–fluid interface so close to the moving contact line that it cannot accurately be measured by low-magnification optical techniques. Instead of attempting to measure the *actual* contact angle with a protractor and an enlarged photograph of the meniscus (the technique used by Rose & Heins, 1962), they report their experimental findings (Hansen & Toong 1971*a*) in terms of an apparent contact angle, $\theta_M$, which is unambiguously defined in terms of $H$, the distance between the apex of the meniscus and the plane containing the moving contact line:

$$\theta_M \equiv \cos^{-1}\left[\frac{-2H/a}{1+(H/a)^2}\right]. \tag{1.2}$$

If the interface were shaped like a portion of a sphere of radius $a/\cos\theta_M$ all the way up to the contact line, then the angle formed between it and the capillary would be $\theta_M$. Using his own data and that of others for the displacement of air by various oils through a glass capillary, Hoffman (1975) has demonstrated graphically that the

† Yarnold includes an extra term in his analysis to account for some of the end effects; however, it does not improve the accuracy.

parameters $\theta_M$, $U\mu/\gamma$, and the static contact angle, $\theta_s$, can be related by a single curve. Jiang, Oh & Slattery (1979) have found that the following function best fits this curve:

$$\frac{\cos\theta_s - \cos\theta_M}{1+\cos\theta_s} = \tanh 4{\cdot}96 Ca^{0{\cdot}702}.$$

Even though Hansen & Toong and Hoffman realized that $\theta_M$ was not the actual contact angle, they did not recognize the fact that such an angle might not be a material property of the system, i.e. it might depend explicitly on the overall geometry of the fluid. If this is the case, then the usefulness of their experimental data is limited. For example, it would not be possible to use $\theta_M$ for studying the spreading of the same liquid over the same solid in any geometry other than the capillary. Hence, in order to extract material invariant information from these experiments, it is essential to perform a detailed analysis of the motion of the fluid in the immediate vicinity of the fluid–fluid interface and the moving contact line.

Unfortunately, this is not a straightforward task. Dussan V. & Davis (1974) have shown that the flow field surrounding a moving contact line, modelled as a continuum with the no-slip boundary condition imposed at a rigid solid wall and with an impermeable fluid–fluid interface, is singular; flow fields having those properties must exert an unbounded force on the solid. Since this implication is unphysical, it is necessary to change at least one of the basic modelling assumptions in order to analyse the motion of the fluid. Several possibilities exist; however, those explored to date all involve introducing a boundary condition which permits the fluid to slip along the wall.

Hocking (1977) and Huh & Mason (1977) have successfully analysed the flow field associated with the displacement of immiscible fluids through a capillary by using various slip boundary conditions to remove the abovementioned singularity. Both have obtained a solution valid for an almost flat fluid–fluid interface near the singular limit, $L_i/a \to 0$, by the method of matched asymptotic expansions. Roughly speaking, $L_i$ denotes the size of the region near the contact line within which the fluid slips along the wall; the no-slip boundary condition, corresponding to $L_i/a \equiv 0$, represents the singular limit. Hocking analysed the case of two immiscible fluids with arbitrary viscosities in which the relative speed of the fluid at the wall is assumed to be proportional to the shear stress exerted by the fluid on the wall. His main conclusion, based on a seemingly reasonable guess for the size of the unknown slip coefficients appearing in his analysis, was that the magnitude of the force exerted by the fluid near the moving contact line is small when compared with the total drag on a capillary over 100 radii in length. However, a detailed analysis was not necessary to come to this conclusion. We already know from (1.1) that the *maximum* effect that the dynamics of the fluid near the moving contact line can have on the pressure drop down the capillary is $2\gamma/a$. Hence, an estimate of its relative importance is given by the expression

$$(2\gamma/a)\,(8U[\mu_A L_A + \mu_R L_R]/a^2)^{-1},$$

the evaluation of which does not require guessing the value of any unknown parameters. Hocking neither analysed the first correction to the shape of the interface nor did he present his solution for the velocity and pressure fields. Huh & Mason (1977) carried Hocking's analysis one step further by solving for the shape of the fluid interface when viscosity of one of the fluids is negligible. They investigate two slip boundary conditions: that used by Hocking, plus a second wherein the fluid exerts no tangential

stress on the solid within a given small distance from the contact line, and does not slip on the solid elsewhere. Their major difficulty arises from the fact that the expression they derive for the apparent contact angle contains *two* unknown parameters: the slip coefficient and the dynamic value of the actual contact angle. Consequently, when comparing their results with experiments they make two unjustified assumptions: the coefficient is $10^{-9}$ m; and the actual contact angle, under dynamic conditions, does not differ from its value at static equilibrium.†

In § 2 it is pointed out, based upon results of existing analyses of flow fields containing moving contact lines, that the motion of the fluid in the outer region, the region of major concern to fluid-mechanicians, can be completely determined in terms of only *one* experimentally measurable parameter. This parameter can be used for the same fluids spreading on the same solid material in any geometry. In § 3 the lowest-order outer problems are formulated, with this in mind, for immiscible fluid displacement through a capillary. Solutions are obtained in §§ 4 and 5 for the lowest-order velocity and pressure field and shape of the fluid–fluid interface for the case of two immiscible fluids with arbitrary viscosities using a technique particularly well suited for moving contact line problems, which differs from that used by Hocking. In § 6 expressions are derived for the various dynamic contact angles which have appeared in capillary flow studies. Finally, in § 7, it is shown how the parameter introduced in § 2 can be determined from existing data of the dynamic behaviour of the apparent contact angle measured in capillaries.

## 2. Approach

One of the major contributions of Hocking and Huh & Mason is the demonstration that flow fields containing moving contact lines can be analysed near the singular limit, $L_i/L_\phi \to 0$, by the method of matched asymptotic expansions. Two regions emerge: the *inner region*, located in the immediate vicinity of the moving contact line and scaled by $L_i$, within which the details of the flow field are very sensitive to the form of the slip boundary condition; and the *outer region*, everywhere else and scaled by $L_\phi$, within which, to lowest order, the fluid satisfies the no-slip boundary condition and the geometry of the fluid plays an important role. Although these analyses can predict the behaviour of experimentally measurable quantities, for example the pressure drop across the capillary and the dynamic behaviour of the apparent contact angle, they have two principal drawbacks: (i) no model for the slip boundary condition has been demonstrated to date to be correct for any given circumstance, (ii) the dynamic behaviour of the actual contact angle is unknown. The key to proceeding further in a quantitative fashion lies in identifying the mechanism by which the inner and outer solutions affect each other.

Upon examining the analyses of Hocking (1977), Huh & Mason (1977), Dussan V. (1976) and Greenspan (1978),‡ we find two features in common. (i) The velocity fields are 'prematched', i.e. to lowest order in $L_i/L_\phi$ there are no non-zero constants to be determined by matching the inner and outer velocity fields [when domain perturba-

† Hocking's results contain only one parameter, the slip coefficient, because he makes the *ad hoc* assumption that the actual contact angle is exactly 90°.

‡ Even though the analyses of Dussan V. and Greenspan do not involve a perturbation in $L_i/L_\phi$, the following remarks are true if their analyses are viewed from this perspective.

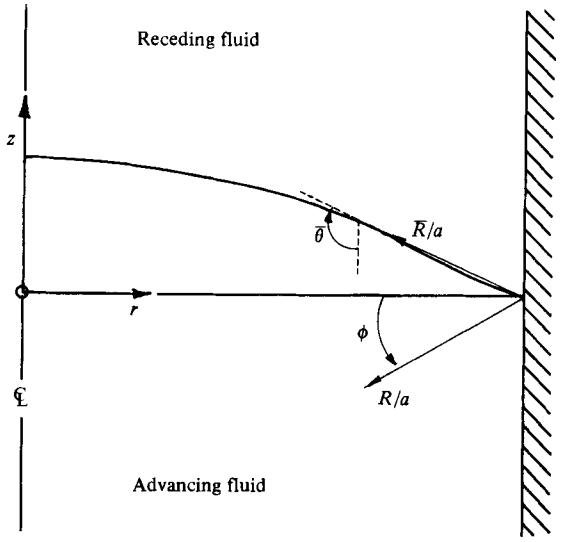


FIGURE 2. Two co-ordinate systems are used: $(r, z)$ and $(R/a, \phi)$. The angle formed between the plane tangent to the interface at a distance $\bar{R}$ from the contact line and the plane tangent to the wall is denoted by $\bar{\theta}$.

tion is used, the velocity field in the intermediate region is that given by Huh & Scriven (1971)]. In this sense, one can say that the velocity field in the outer region is not directly affected by what happens near the moving contact line. (ii) The slope of the fluid–fluid interface in the outer region can be completely determined except for a constant of integration. Knowledge of this constant is equivalent to knowing the angle of inclination of the interface, $\bar{\theta}$, at a specific distance from the contact line, $\bar{R}$; refer to figure 2.

If the outer solution is valid in the neighbourhood of the contact line then the abovementioned constant can be determined from the dynamic behaviour of the actual contact angle ($\bar{\theta}$ is the actual contact angle when $\bar{R} = 0$). However, it is not; hence the constant must be determined by matching the inner and outer solutions for the slope of the interface. It is only through the slope of the interface that the motion of the fluids in the outer region is affected by the dynamics of the fluids in the inner region in the abovementioned analyses.

In other words, if $\bar{\theta}$ at $\bar{R}$ is known then the entire solution in the outer region can be calculated completely. *If $\bar{R}$ is chosen to be a specific position within the intermediate region, the region where both inner and outer solutions are valid, then $\bar{\theta}$ must have the property that it is independent of the overall geometry of the outer region* ($\theta_{\mathrm{I}}$ and $R_{\mathrm{I}}$ will denote the value of $\bar{\theta}$ and $\bar{R}$ at a specific position in the intermediate region). If the proper model for the dynamic behaviour of the fluids in the inner region were known, then the value of $\theta_{\mathrm{I}}$ could be calculated by first principles through matching. However, such knowledge does not seem to be forthcoming in the foreseeable future. One of our main objectives is pointing out that this does not present an obstacle to fluid-mechicians interested in predicting the spreading of liquids on solid surfaces. It will be shown how to determine $\theta_{\mathrm{I}}$ empirically from experimental measurements of immiscible fluid displacement through a capillary. The capillary can thus be viewed as a device

from which basic information can be obtained that characterizes the spreading of liquids on solid surfaces.

The *key* to the correctness of using this procedure to solve the outer problem in terms of $\theta_I$ lies in the *assumption* that *all* models of the inner region, not just the ones cited at the beginning of this section, give rise to a velocity field in the inner region that 'prematch' that of the outer region. Although the models of the inner region from which this assumption has been abstracted all involve introducing a slip boundary condition, they do in fact reflect vastly different physical mechanisms (refer to Dussan V. 1979, for a detailed discussion).

## 3. The outer region

The geometry and co-ordinate system are shown in figure 2. The frame of reference is chosen so that the fluid–fluid interface is stationary, the walls of the capillary moving with a velocity of $-U\hat{\mathbf{z}}$. It is assumed that the dimensionless Navier–Stokes equations are satisfied within both fluids:

$$C_a Re_K \left[u^K \frac{\partial u^K}{\partial r} + w^K \frac{\partial u^K}{\partial z}\right] = -\frac{\partial p^K}{\partial r} + \bar{\mu}_K C_a \left[\frac{\partial}{\partial r}\left(\frac{1}{r}\frac{\partial}{\partial r}(ru^K) + \frac{\partial^2 u^K}{\partial z^2}\right)\right],$$

$$C_a Re_K \left[u^K \frac{\partial w^K}{\partial r} + w^K \frac{\partial w^K}{\partial z}\right] = -\frac{\partial p^K}{\partial z} + \bar{\mu}_K C_a \left[\frac{1}{r}\frac{\partial}{\partial r}\left(r\frac{\partial w^K}{\partial r}\right) + \frac{\partial^2 w^K}{\partial z^2}\right],$$

where $K = A, R$ denotes the advancing and receding fluids, respectively; $u$ and $w$ are the radial and axial velocity components; and $p + \rho g a^2 z/\gamma$ is the pressure within the vertical capillary. Each fluid must also satisfy the continuity equation:

$$\frac{1}{r}\frac{\partial}{\partial r}(ru^K) + \frac{\partial w^K}{\partial z} + \ = 0.$$

The outer flow field satisfies the no-slip boundary condition along the moving wall, so that

$$u^K = 0, \quad w^K = -1 \quad \text{at} \quad r = 1, \quad |z| < \infty$$

and if the height of the fluid–fluid interface is given by a radial function, $h(r)$, then the normal component of the velocity must be zero:

$$-u^K \frac{dh}{dr} + w^K = 0 \quad \text{at} \quad z = h(r), \quad r \leqslant 1,$$

while the tangential component of the velocity is the same in both fluids:

$$\left[\!\left[u + w\frac{dh}{dr}\right]\!\right] = 0 \quad \text{at} \quad z = h(r), \quad r \leqslant 1,$$

where the brackets are defined by

$$[\![g(r)]\!] \equiv \lim_{\epsilon \to 0} \{g^A(r, h-\epsilon) - g^R(r, h+\epsilon)\},$$

$g(r, z)$, represents any scalar field which characterizes the behaviour of the advancing and receding fluids such as pressure and either component of the velocity vector. The

dynamic boundary condition requires first that the tangential stress exerted by either fluid upon the meniscus be the same,

$$\left[\left[\frac{dh}{dr}\left(\frac{\partial w}{\partial z}-\frac{\partial u}{\partial r}\right)+\left(1-\left(\frac{dh}{dr}\right)^2\right)\left(\frac{\partial u}{\partial z}+\frac{\partial w}{\partial r}\right)\right]\right]=0 \quad \text{at} \quad z=h(r), \quad r\leqslant 1,$$

and second that the interface have a shape such that the product of its curvature and surface tension balance the normal stress difference,

$$\frac{d^2h}{dr^2}\Big/\left(1+\left(\frac{dh}{dr}\right)^2\right)^{\frac{3}{2}}+\frac{1}{r}\frac{dh}{dr}\Big/\left(1+\left(\frac{dh}{dr}\right)^2\right)^{\frac{1}{2}}=-[\![p]\!]+Bz$$

$$+2C_a\left[\left[\bar{\mu}\left\{\left(\frac{dh}{dr}\right)^2\frac{\partial u}{\partial r}-\frac{dh}{dr}\left(\frac{\partial u}{\partial z}+\frac{\partial w}{\partial r}\right)+\frac{\partial w}{\partial z}\right\}\right]\right]\Big/\left(1+\left(\frac{dh}{dr}\right)^2\right) \quad \text{at} \quad z=h(r).$$

The boundary conditions on $h(r)$ are

$$h(1)=0 \quad \text{and} \quad \frac{dh}{dr}=\tan\left(\frac{\pi}{2}-\theta_{\mathrm{I}}\right) \quad \text{at} \quad r=1-\frac{R_{\mathrm{I}}}{a},$$

where $\theta_{\mathrm{I}}$ and $R_{\mathrm{I}}$ have already been defined in § 2. We shall treat $\theta_{\mathrm{I}}$ as a known property of the system. Other parameters appearing in the above equations are: the capillary number, $C_a \equiv U\mu_A/\gamma$; the Bond number, $B \equiv (\rho_A-\rho_R)ga^2/\gamma$, where $\rho_A$ and $\rho_R$ are fluid densities; the Reynolds numbers, $Re_K \equiv Ua\rho_K/\mu_K$; and the normalized viscosities, $\bar{\mu}_K \equiv \mu_K/\mu_A$. The *dimensional* form of the dependent and independent variables are

$$p\gamma/a; \quad (uU, wU); \quad (ra, za); \quad R; \quad ha.$$

We shall only be concerned with the case wherein the five parameters ($\theta_{\mathrm{I}}-\frac{1}{2}\pi$, $C_a$, $B$, $Re_A$, $Re_R$) are small. Under these circumstances it is anticipated that $h(r)$ is everywhere close to the plane $z=0$. It is reasonable to expect that the velocity and pressure field, or the continuation of each field, has the property that a Taylor series expansion at $z=0$ can be used to express values of the dependent variables at $z=h(r)$ (domain perturbation). For example, the kinematic boundary condition at the fluid–fluid interface becomes

$$w^K+\frac{\partial w^K}{\partial z}h+\frac{\partial^2 w^K}{\partial z^2}\frac{h^2}{2}+\ldots-\frac{dh}{dr}\left[u^K+\frac{\partial u^K}{\partial z}h+\frac{\partial^2 u^K}{\partial z^2}\frac{h^2}{2}+\ldots\right]=0 \quad \text{at} \quad z=h(r).$$

Thus all the boundary conditions at the meniscus are transformed to conditions at $z=0$. The fluid–fluid interface remains at $z=h(r)$.

It is assumed that the dependent variables ($u^K$, $w^K$, $p^K$, $h$) can everywhere be described by an asymptotic expansion valid in the limit that the five parameters approach zero:

$$\begin{pmatrix}u^K\\w^K\\p^K\\h\end{pmatrix}\sim\begin{pmatrix}u_0^K\\w_0^K\\p_0^K\\h_0\end{pmatrix}+(\tfrac{1}{2}\pi-\theta_{\mathrm{I}})\begin{pmatrix}u_\theta^K\\w_\theta^K\\p_\theta^K\\h_\theta\end{pmatrix}+C_a\begin{pmatrix}u_{C_a}^K\\w_{C_a}^K\\p_{C_a}^K\\h_{C_a}\end{pmatrix}+B\begin{pmatrix}u_B^K\\w_B^K\\p_B^K\\h_B\end{pmatrix}+Re_A\begin{pmatrix}u_{Re_A}^K\\w_{Re_A}^K\\p_{Re_A}^K\\h_{Re_A}\end{pmatrix}+Re_R\begin{pmatrix}u_{Re_R}^K\\w_{Re_R}^K\\p_{Re_R}^K\\h_{Re_R}\end{pmatrix}+\ldots.$$

This expansion is substituted into each governing equation and boundary condition to create a sequence of well-posed boundary value problems.

To lowest order, the pressure field and interface shape must satisfy

$$\nabla p_0^K = 0;$$

$$\frac{1}{r}\frac{d}{dr}\left(r\frac{dh_0}{dr}\right) = p_0^R - p_0^A \quad \text{at} \quad z = 0;$$

$$\frac{dh_0}{dr} = 0 \quad \text{at} \quad r = 1 - R_I/a; \quad \text{and} \quad h_0 = 0 \quad \text{at} \quad r = 1.$$

The solution to the above is

$$h_0 \equiv 0 \quad \text{and} \quad p_0^A \equiv p_0^R \,(\text{constant}).$$

In a similar manner it can be shown that

$$\{p_\alpha^A = p_\alpha^R = h_\alpha = 0 \,|\, \alpha = B, Re_A, Re_R\}.$$

The terms $p_\theta^K$ and $h_\theta$ must satisfy

$$\nabla p_\theta^K = 0;$$

$$\frac{1}{r}\frac{d}{dr}\left(r\frac{dh_\theta}{dr}\right) = p_\theta^R - p_\theta^A \quad \text{at} \quad z = 0;$$

$$\frac{dh_\theta}{dr} = 1 \quad \text{at} \quad r = 1 - R_I/a; \quad \text{and} \quad h_\theta = 0 \quad \text{at} \quad r = 1.$$

The solution is

$$h_\theta = \tfrac{1}{2}(r^2 - 1) \quad \text{and} \quad p_\theta^A = p_\theta^R - 2 \quad (\text{constants}).\dagger$$

This mode, while free of viscous effects in the outer region, nevertheless represents a dynamic contribution to the interfacial shape and pressure field since the value of $\theta_I$ depends on the speed of the contact line. The lowest-order mode in which viscous effects are important is described by

$$0 = -\frac{\partial p_{Ca}^K}{\partial r} + \bar{\mu}_K\left[\frac{\partial}{\partial r}\left(\frac{1}{r}\frac{\partial}{\partial r}(ru_0^K) + \frac{\partial^2 u_0^K}{\partial z^2}\right]\right.,$$

$$0 = -\frac{\partial p_{Ca}^K}{\partial z} + \bar{\mu}_K\left[\frac{1}{r}\frac{\partial}{\partial r}\left(r\frac{\partial w_0^K}{\partial r}\right) + \frac{\partial^2 w_0^K}{\partial z^2}\right], \tag{3.1}$$

and

$$\frac{1}{r}\frac{\partial}{\partial r}(ru_0^K) + \frac{\partial w_0^K}{\partial z} = 0,$$

with boundary conditions

$$u_0^K = 0 \quad \text{and} \quad w_0^K = 1 \quad \text{at} \quad r = 1,$$

$$w_0^K = 0, \quad u_0^A = u_0^R, \quad \text{and} \quad \bar{\mu}_A\frac{\partial u_0^A}{\partial z} = \bar{\mu}_R\frac{\partial u_0^R}{\partial z} \quad \text{at} \quad z = 0,$$

$$\frac{1}{r}\frac{d}{dr}\left(r\frac{dh_{Ca}}{dr}\right) = p_{Ca}^R - p_{Ca}^A + 2\left[\bar{\mu}_A\frac{\partial w_0^A}{\partial z} - \bar{\mu}_R\frac{\partial w_0^R}{\partial z}\right] \quad \text{at} \quad z = 0,$$

and $dh_{Ca}/dr = 0$ at $r = 1 - R_I/a$, and $h_{Ca} = 0$ at $r = 1$. In the next section, a solution is obtained for $u_0^K$ and $w_0^K$ which is then used to obtain $p_{Ca}^K$ and $h_{Ca}$.

† A negligible error has been introduced by neglecting terms involving $R_I/a$.

## 4. The outer velocity field

### 4.1. *Solution*

It is convenient to introduce a stream function, $\psi^K$:

$$(u_0^K, w_0^K) = \left(\frac{1}{r}\frac{\partial \psi^K}{\partial z}, -\frac{1}{r}\frac{\partial \psi^K}{\partial r}\right).$$

In terms of the stream function, the governing equation and boundary conditions for the lowest-order mode in which viscous effects are important become

$$\left[r\frac{\partial}{\partial r}\frac{1}{r}\frac{\partial}{\partial r}+\frac{\partial^2}{\partial z^2}\right]^2 \psi^K = 0;$$

$$\psi^K = 0, \quad \frac{\partial \psi^K}{\partial r} = 1 \quad \text{at} \quad r = 1,$$

$$\psi^K = 0, \quad \frac{\partial \psi^A}{\partial z} = \frac{\partial \psi^R}{\partial z}, \quad \bar{\mu}_A \frac{\partial^2 \psi^A}{\partial z^2} = \bar{\mu}_R \frac{\partial^2 \psi^R}{\partial z^2} \quad \text{at} \quad z = 0.$$

It is also convenient to solve this system by superposition:

$$\psi^K = \psi_{\mathrm{I}}^K + \frac{1}{\bar{\mu}_K}\frac{\bar{\mu}_A \bar{\mu}_R}{\bar{\mu}_A + \bar{\mu}_R}\psi_{\mathrm{II}}^K$$

with the non-homogeneous boundary condition at $r = 1$ absorbed in $\psi_{\mathrm{I}}^K$:

$$\psi_{\mathrm{I}}^K = 0, \quad \frac{\partial \psi_{\mathrm{I}}^K}{\partial r} = 1 \quad \text{at} \quad r = 1$$

$$\psi_{\mathrm{I}}^K = 0, \quad \frac{\partial^2 \psi_{\mathrm{I}}^K}{\partial z^2} = 0 \quad \text{at} \quad z = 0.$$

The solution for $\psi_{\mathrm{I}}^K$ was obtained by Bhattacharjii & Savic (1965) using a sine transformation:

$$\psi_{\mathrm{I}}^K = (-1)^{K-1}\frac{2}{\pi}\int_0^\infty \left\{\frac{rI_1(rs)\,I_0(s) - r^2 I_0(rs)\,I_1(s)}{2I_0(s)\,I_1(s) - sI_0^2(s) + sI_1^2(s)}\right\}\frac{\sin(zs)}{s}\,ds.\ddagger \tag{4.1}$$

Note that this flow exhibits no tangential stress at $z = 0$. The functions $I_0$ and $I_1$ are modified Bessel functions as given in Abramowitz & Stegun (1964).

The function $\psi_{\mathrm{II}}^K$ has boundary conditions

$$\psi_{\mathrm{II}}^K = 0 \quad \text{and} \quad \frac{\partial \psi_{\mathrm{II}}^K}{\partial r} = 0 \quad \text{at} \quad r = 1;$$

$$\psi_{\mathrm{II}}^K = 0, \quad \left[\!\left[\frac{1}{\bar{\mu}}\left(\frac{\bar{\mu}_A \bar{\mu}_R}{\bar{\mu}_A + \bar{\mu}_R}\right)\frac{1}{r}\frac{\partial \psi_{\mathrm{II}}}{\partial z}\right]\!\right] = -\left[\!\left[\frac{1}{r}\frac{\partial \psi_{\mathrm{I}}}{\partial z}\right]\!\right] \quad \text{and} \quad \frac{\partial^2 \psi_{\mathrm{II}}^A}{\partial z^2} = \frac{\partial^2 \psi_{\mathrm{II}}^R}{\partial z^2} \quad \text{at} \quad z = 0.$$

A general solution for $\psi_{\mathrm{II}}$† in either fluid can be found by separation of variables or in

† It will be established shortly that the superscript $K$ is not necessary for $\psi_{\mathrm{II}}$.

‡ Where $(-1)^{A-1} \equiv -1$ and $(-1)^{R-1} \equiv +1$.

| $n$ | Re $s_n$ | Im $s_n$ | Re $C(s_n)$ | Im $C(s_n)$ |
|---|---|---|---|---|
| 0 | 0·0 | 0·0 | 0·0 | 0·0 |
| 1 | 1·46746 | 4·46630 | −9·9816 | −0·5600 |
| 2 | 1·72697 | 7·69410 | −17·3266 | −4·1056 |
| 3 | 1·89494 | 10·87457 | −24·4043 | −7·9430 |
| 4 | 2·02006 | 14·03889 | −31·3717 | −11·9077 |
| 5 | 2·11995 | 17·19556 | −38·2801 | −15·9442 |
| 6 | 2·20312 | 20·34795 | −45·1530 | −20·0260 |
| 7 | 2·27440 | 23·49770 | −52·0046 | −24·1381 |
| 8 | 2·33678 | 26·64571 | −58·8325 | −28·2742 |
| 9 | 2·39222 | 29·79247 | −65·6508 | −32·4293 |
| 10 | 2·44212 | 32·93831 | −72·4559 | −36·5938 |
| 11 | 2·48750 | 36·08350 | −79·2564 | −40·7747 |
| 12 | 2·52911 | 39·22815 | −86·0456 | −44·9601 |
| 13 | 2·56752 | 42·37238 | −92·8238 | −49·1582 |
| 14 | 2·60319 | 45·51630 | −99·6144 | −53·3514 |
| 15 | 2·63648 | 48·65990 | −106·3922 | −57·5685 |
| 16 | 2·66769 | 51·80330 | −113·1692 | −61·7704 |
| 17 | 2·69706 | 54·94652 | −119·9416 | −65·9903 |
| 18 | 2·72481 | 58·08954 | −126·7092 | −70·2071 |
| 19 | 2·75110 | 61·23247 | −133·4834 | −74·4356 |
| 20 | 2·77609 | 64·37526 | −140·2406 | −78·6654 |

TABLE 1. Eigenvalues and eigenfunction coefficients.

terms of a Green's function. Work by Smith (1952) and, later, Yoo & Joseph (1977) suggests a separation of variables of the form

$$\begin{Bmatrix} \dfrac{\partial^2 \psi_{\mathrm{II}}}{\partial z^2} \\ r\dfrac{\partial}{\partial r}\left(\dfrac{1}{r}\dfrac{\partial}{\partial r}\psi_{\mathrm{II}}\right) \end{Bmatrix} = \sum_s C(s) \begin{Bmatrix} \rho_1(r;s) \\ \rho_2(r;s) \end{Bmatrix} e^{is|z|} \tag{4.2}$$

where the sets $\{s\}$ and $\{\boldsymbol{\rho}\}$ are eigenvalues and eigenfunctions determined by the boundary conditions at $r = 1$ and the requirement of a bounded velocity field at $r = 0$. Each element of $\{s\}$ must be a zero of the characteristic function $g(s)$:

$$g(s) \equiv 2I_0(s)\,I_1(s) - sI_0^2(s) + sI_1^2(s).$$

Those elements with non-negative real and imaginary parts are ordered with increasing magnitude to form $\{s_n\}$, where $s_0 = 0$; the complete set of eigenvalues which has the required property that $e^{is|z|}$ is bounded for large $z$ consists of $\{s_n\} \cup \{-\overline{s_n}\}$. It can be shown for large $n$ that $s_n \sim \frac{1}{2}\ln 4\pi(n+\frac{1}{2}) + \pi i(m+\frac{1}{2})$. The values of $\{s_n : n = 1, \ldots, 400\}$ were found by the secant method applied to the analytic function $g(s)$ and the first twenty-one are listed in table 1. Zeros near the origin were counted by numerically integrating $g'/g$ about closed contours to confirm that no element of $\{s_n\}$ was missed.

A sequence of functions, $\{\boldsymbol{\sigma}(r;s)\}$, biorthogonal to $\{\boldsymbol{\rho}(r;s)\}$ have been found with the property that if $s$ and $s'$ are any two eigenvalues then

$$\int_0^1 \boldsymbol{\sigma}(r;s) \begin{bmatrix} 0 & -1 \\ 1 & 2 \end{bmatrix} \boldsymbol{\rho}(r;s')\, d\ln r = \begin{cases} 0 & \text{if } s \neq s', \\ k(s) & \text{if } s = s'. \end{cases}$$

The constants $C(s_n)$ are then determined by

$$C(s_n) = \frac{1}{k(s_n)} \int_0^1 \boldsymbol{\sigma}(r; s_n) \begin{bmatrix} 0 & -1 \\ 1 & 2 \end{bmatrix} \begin{bmatrix} \dfrac{\partial^2 \psi_{\mathrm{II}}}{\partial z^2} \\ r \dfrac{\partial}{\partial r}\left(\dfrac{1}{r}\dfrac{\partial \psi_{\mathrm{II}}}{\partial r}\right) \end{bmatrix}\Bigg|_{z=0} d\ln r, \tag{4.3}$$

where

$$\boldsymbol{\sigma} = (\sigma_1, \sigma_2) = (2\rho_1(r;s) + \rho_2(r;s), \rho_1(r;s)),$$

$$\boldsymbol{\rho} = \begin{pmatrix} \rho_1 \\ \rho_2 \end{pmatrix} = \begin{pmatrix} rI_1(rs)/I_1(s) - r^2 I_0(rs)/I_0(s) \\ 2rI_1(rs)/sI_0(s) - rI_1(rs)/I_1(s) + r^2 I_0(rs)/I_0(s) \end{pmatrix},$$

exhibiting the properties that $\boldsymbol{\rho}(r;s) = \boldsymbol{\rho}(r;-s)$ and $\boldsymbol{\rho}(r;s) = \overline{\boldsymbol{\rho}(r;\bar{s})}$. In addition, it can be shown that $k(s) = -I_1^2(s)/s_2 I_0^2(s)$ for $s = s_n$. For the problem at hand, $\psi_{\mathrm{II}}$ and

$$r \frac{\partial}{\partial r}\left(\frac{1}{r}\frac{\partial \psi_{\mathrm{II}}}{\partial r}\right)$$

are identically zero on $z = 0$, so that (3.2) can be integrated to give

$$\psi_{\mathrm{II}} = -2 \sum_{m=1}^{\infty} \mathrm{Re}\left\{\frac{C(s_n)}{s_n^2} \rho_1(r; s_n)\, e^{is_n|z|}\right\}, \tag{4.4}$$

where the $C(s_n)$ can be calculated for any specified $\partial^2\psi_{\mathrm{II}}/\partial z^2|_{z=0}$. Since $\partial^2\psi_{\mathrm{I}}/\partial z^2 = 0$ on $z = 0$, the function $\tau(r) = (1/r)\partial^2\psi_{\mathrm{II}}/\partial z^2|_{z=0}$ represents the entire tangential stress on $z = 0$. This is the same in both fluids, which justifies the removal of the superscript from $\psi_{\mathrm{II}}$.

All that remains is to calculate $\tau$. Upon combining (4.2), (4.3) and (4.4) it is found that $\tau$ must satisfy:

$$A(r;\tau) = \frac{2}{r}\frac{\partial \psi_{\mathrm{I}}^R}{\partial z}\Bigg|_{z=0}, \tag{4.5}$$

where

$$A(r;\tau) \equiv \lim_{|z|\to 0} 2 \sum_{n=1}^{\infty} \mathrm{Re}\left\{\frac{\rho_1(r;s_n)\, e^{is_n|z|}}{is_n\, k(s_n)} \int_0^1 \tau(r')\, \rho_1(r';s_n)\, dr'\right\}.$$

Equation (4.5) is solved approximately by assuming $\tau$ has the form

$$\tau \doteq \tau^M(r) = \frac{-32}{\pi^2 - 4}\left(\frac{r}{1-r^2}\right) + \sum_{m=1}^{M} \alpha_m^M r^{2m-1}.$$

The first term on the right-hand side of the equation represents the anticipated *singular* behaviour which $\tau$ must have near the contact line in order for the velocity field in the outer region to 'prematch' that of the inner as discussed in § 2.

The sets of coefficients $\{\alpha_m^M : m = 1, \ldots, M\}$ for different values of $M$ were obtained by substituting the above expression for $\tau$ into (4.5) and minimizing a numerical approximation to the $\mathscr{L}^2$ norm of the residue:

$$\frac{\partial}{\partial \alpha_m^M} \sum_{P=1}^{39} \left\{\frac{2}{0{\cdot}025P}\frac{\partial \psi_{\mathrm{I}}^R}{\partial z}\Bigg|_{\substack{z=0 \\ r=0{\cdot}025P}} - A(0{\cdot}025P;\tau)\right\}^2 = 0 \quad \text{for} \quad m = 1, \ldots, M. \tag{4.6}$$

The difference between the left- and right-hand sides of (4.5) corresponding to a discontinuity in the radial component of the velocity at $z = 0$, $[\![u_0]\!]|_{z=0}$, for $M = 1, 2, 3, 4$

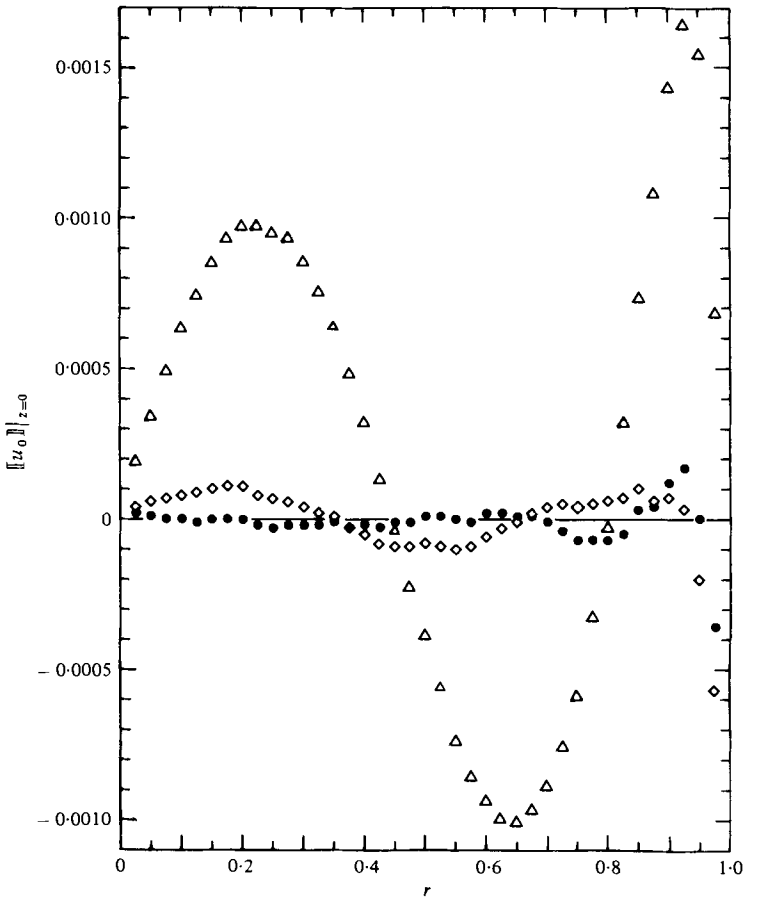


FIGURE 3. The magnitude of the discontinuity in the tangent component of the velocity at the interface, $[\![u_0]\!]_{z=0}$, decreases in value as the number of trial functions increases in number; curves △, ◇ and ● correspond to two, three and four trial functions, respectively.

is illustrated in figure 3. As $M$ increases in value, the error *uniformly* approaches zero. This is also illustrated by the behaviour of $\tau^M - \tau^4$ in figure 4, where

$$\tau^4 \doteq \frac{-5{\cdot}452r}{1-r^2} - 4{\cdot}860r + 1{\cdot}336r^3 + 1{\cdot}063r^5 - 0{\cdot}348r^7. \tag{4.7}$$

The corresponding values of $\{C(s_n)\}$, which are the same for both fluids, appear in table 1. The radial velocity of the fluid at $z = 0$, $u_0^A(r, 0)$, can readily be calculated from its definition:

$$u_0^A(r,0) = u_0^R(r,0) = \frac{1}{r}\frac{\partial \psi_{\mathrm{I}}^R}{\partial z}\bigg|_{z=0} + \frac{\bar{\mu}_A}{\bar{\mu}_A + \bar{\mu}_R}\frac{1}{r}\frac{\partial \psi_{\mathrm{II}}^R}{\partial z}\bigg|_{z=0}$$

along with the identity

$$\frac{1}{r}\frac{\partial \psi_{\mathrm{II}}^K}{\partial z}\bigg|_{z=0} = -\frac{2}{r}\frac{\partial \psi_{\mathrm{I}}^K}{\partial z}\bigg|_{z=0}$$

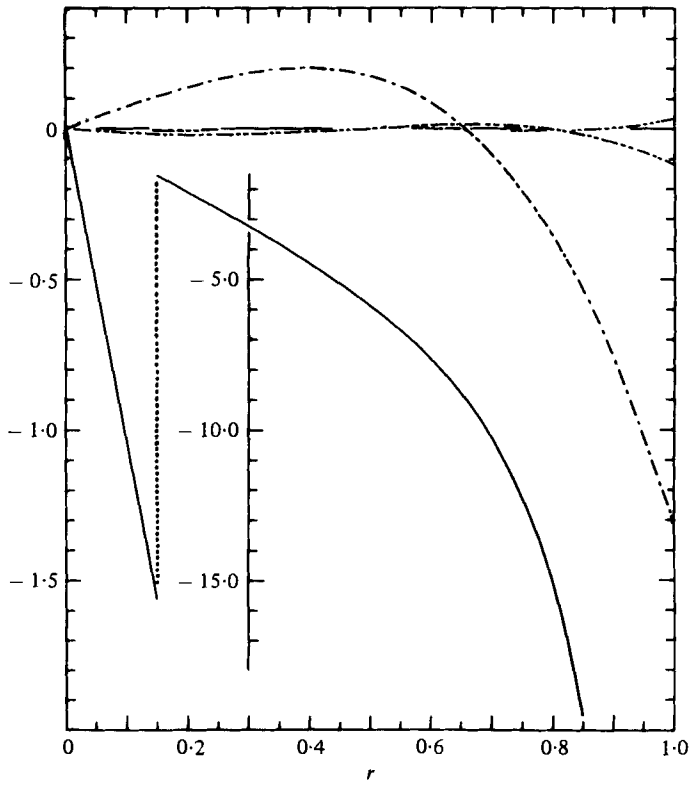


FIGURE 4. The solid line —— corresponds to the tangent component of the surface traction vector evaluated at the fluid–fluid interface when four trial functions are used, $\tau_4$; —·—, $\tau^1 - \tau^4$; —··—, $\tau^2 - \tau^4$; —···—, $\tau^3 - \tau^4$.

and an evaluation of $\partial\psi_{\mathrm{I}}^R/\partial z|_{z=0}$ obtained from (4.1):

$$-\frac{1}{r}\frac{\partial\psi_{\mathrm{I}}^R}{\partial z}\bigg|_{z=0} \doteq 1{\cdot}0168r - 0{\cdot}3206r^3 - 0{\cdot}0561r^5 + 0{\cdot}0225r^7 - 0{\cdot}0259r^9.$$

The above expression is accurate to within an absolute error of 0·0003, or 0·05 % of its maximum value.

An integral representation of $\psi_{\mathrm{II}}$ was also obtained by finding the Green's function, see appendix A. This form, though somewhat cumbersome, was useful in evaluating properties of the solution at $z = 0$, where the sum of the eigenfunctions shows poor convergence. In addition, a grid of $\psi_{\mathrm{I}}$ and $\psi_{\mathrm{II}}$ values is displayed in table 2; this may be used to estimate velocities at any point within the two fluids.

### 4.2. *Discussion*

The streamlines within the receding fluid are shown in figure 5 for both large and small values of $\bar{\mu}_R$. It is interesting to note that a stagnation point is predicted *within* the less viscous fluid along the axis at a distance $z_s = 0$ from the flat interface. Figure 6 gives the dependence of $z_s$ on the viscosity ratio; note that its largest value, $z_s \doteq 0{\cdot}25$,

$\psi_{\mathrm{I}}$

| $r$ \ $z$ | 0·10 | 0·20 | 0·30 | 0·40 | 0·50 | 0·60 | 0·70 | 0·80 | 0·90 | ∞ |
|---|---|---|---|---|---|---|---|---|---|---|
| 0·10 | −0·00100 | −0·00193 | −0·00274 | −0·00338 | −0·00390 | −0·00426 | −0·00452 | −0·00469 | −0·00479 | −0·00495 |
| 0·20 | −0·00396 | −0·00763 | −0·01079 | −0·01333 | −0·01526 | −0·01664 | −0·01760 | −0·01823 | −0·01864 | −0·01920 |
| 0·30 | −0·00876 | −0·01681 | −0·02364 | −0·02904 | −0·03306 | −0·03590 | −0·03783 | −0·03908 | −0·03987 | −0·04095 |
| 0·40 | −0·01517 | −0·02893 | −0·04024 | −0·04910 | −0·05544 | −0·05981 | −0·06270 | −0·06455 | −0·06569 | −0·06720 |
| 0·50 | −0·02286 | −0·04313 | −0·05932 | −0·07125 | −0·07953 | −0·08502 | −0·08855 | −0·09074 | −0·09208 | −0·09375 |
| 0·60 | −0·03132 | −0·05803 | −0·07808 | −0·09192 | −0·10099 | −0·10673 | −0·11028 | −0·11243 | −0·11370 | −0·11520 |
| 0·70 | −0·03976 | −0·07113 | −0·09230 | −0·10555 | −0·11362 | −0·11842 | −0·12127 | −0·12294 | −0·12388 | −0·12495 |
| 0·80 | −0·04650 | −0·07719 | −0·09424 | −0·10353 | −0·10869 | −0·11159 | −0·11324 | −0·11417 | −0·11468 | −0·11520 |
| 0·90 | −0·04550 | −0·06316 | −0·07016 | −0·07341 | −0·07506 | −0·07594 | −0·07642 | −0·07669 | −0·07683 | −0·07695 |

$\psi_{\mathrm{II}}$

| $r$ \ $z$ | 0·10 | 0·20 | 0·30 | 0·40 | 0·50 | 0·60 | 0·70 | 0·80 | 0·90 | ∞ |
|---|---|---|---|---|---|---|---|---|---|---|
| 0·10 | 0·00154 | 0·00227 | 0·00242 | 0·00222 | 0·00186 | 0·00146 | 0·00109 | 0·00078 | 0·00054 | 0 |
| 0·20 | 0·00608 | 0·00886 | 0·00937 | 0·00854 | 0·00709 | 0·00552 | 0·00409 | 0·00291 | 0·00201 | 0 |
| 0·30 | 0·01329 | 0·01911 | 0·01989 | 0·01783 | 0·01460 | 0·01121 | 0·00821 | 0·00579 | 0·00396 | 0 |
| 0·40 | 0·02262 | 0·03178 | 0·03227 | 0·02825 | 0·02263 | 0·01706 | 0·01230 | 0·00856 | 0·00579 | 0 |
| 0·50 | 0·03318 | 0·04495 | 0·04397 | 0·03719 | 0·02892 | 0·02126 | 0·01502 | 0·01028 | 0·00685 | 0 |
| 0·60 | 0·04355 | 0·05565 | 0·05146 | 0·04148 | 0·03101 | 0·02211 | 0·01524 | 0·01022 | 0·00670 | 0 |
| 0·70 | 0·05127 | 0·05934 | 0·05041 | 0·03807 | 0·02712 | 0·01864 | 0·01250 | 0·00820 | 0·00528 | 0 |
| 0·80 | 0·05149 | 0·04969 | 0·03721 | 0·02588 | 0·01745 | 0·01154 | 0·00751 | 0·00481 | 0·00304 | 0 |
| 0·90 | 0·03333 | 0·02269 | 0·01439 | 0·00916 | 0·00585 | 0·00373 | 0·00236 | 0·00148 | 0·00091 | 0 |

TABLE 2. Stream function component values.

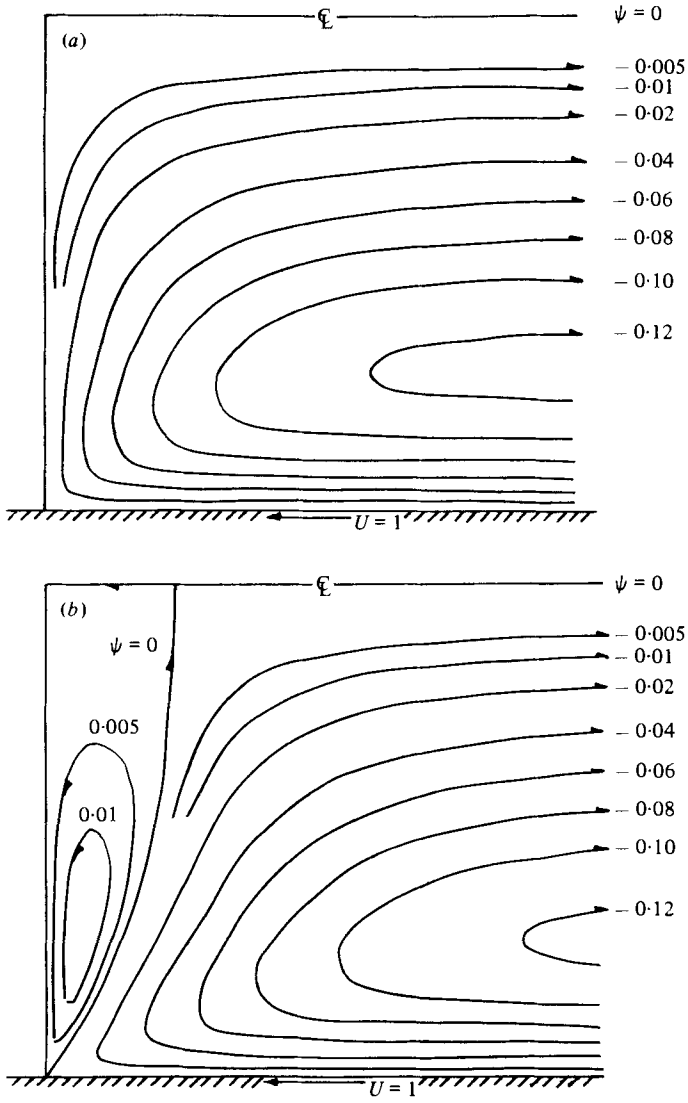


FIGURE 5. Constant streamlines within the receding fluid are given in (*a*) for $\mu_R \gg \mu_A$ and (*b*) for $\mu_R \ll \mu_A$.

occurs in the limit as the viscosity ratio approaches zero. An internal stagnation point of this sort has been observed by Dussan V. (1977) for glycerine displacing mineral oil through a circular tube.

It has been noted by Hocking (1977) that, when the two fluids have the same viscosity, the velocity at $z = 0$ is everywhere zero. The flow field is the same as that occurring when a flat-headed plunger displaces a fluid out of a circular tube. This problem has been solved numerically by Wagner (1975) who represents values of the stream function for $Re = 10$. His values are consistently smaller in magnitude than ours, differing up to 2·3 % along $r = 0{\cdot}5$, and 4·8 % along $z = 0{\cdot}549$. This discrepancy is probably due to the fact that our results correspond to $Re = 0$; although his solution

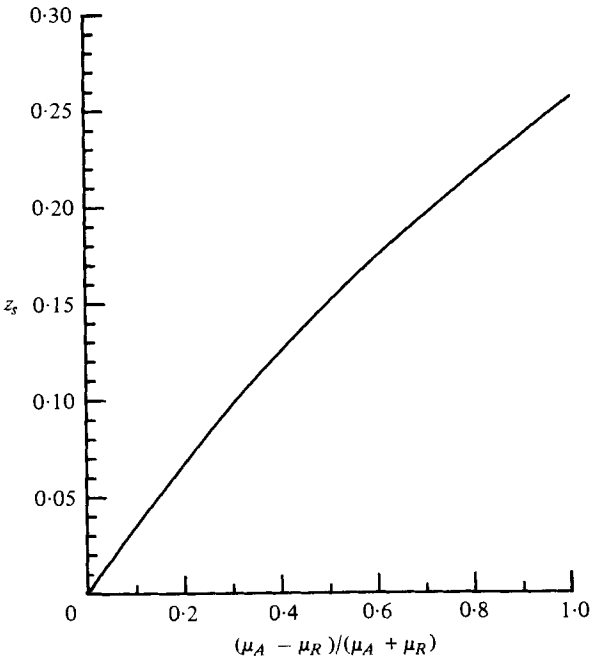


FIGURE 6. A stagnation point is located within the less viscous fluid at $(0, z_s)$.

is clearly in error in the region where the face of the plunger meets the wall (he calculates a finite drag on the wall which should clearly be infinite subject to his assumptions).

Figure 7 gives the difference, at a distance $R = 0{\cdot}05a$ from the contact line, between the velocity field and its anticipated asymptotic form:

$$\mathbf{u}^K = -\frac{a}{R}\frac{\partial \Phi^K}{\partial \phi}\hat{\mathbf{R}} + a\frac{\partial \Phi^K}{\partial R}\hat{\phi},$$

where

$$\frac{a\Phi^K}{R} = \frac{2}{\pi}|\phi|\cos\phi + \frac{1}{\bar{\mu}_K}\frac{\bar{\mu}_A\bar{\mu}_R 4}{(\bar{\mu}_A+\bar{\mu}_R)(\pi^2-4)}\left(\frac{4}{\pi}|\phi|\cos\phi + 2\phi\sin\phi - \pi\sin|\phi|\right). \quad (4.8)$$

This is the solution given by Huh & Scriven (1971); however, they did not recognize that it represented the velocity field of the fluids within the intermediate region. Upon repeated evaluation of the difference at decreasing values of $R$, it is found to be $O(R)$ as $R \to 0$. It has also been established through numerical calculations that

$$\tau(R/a) \doteq \frac{-16}{\pi^2-4} \times \frac{a}{R} - 0{\cdot}08 + O(R/a) \quad \text{as} \quad R/a \to 0$$

and

$$\frac{2}{r}\frac{\partial^2 \psi_{II}^R}{\partial r\,\partial z}\bigg|_{z=0} \doteq 1{\cdot}34 + O(R/a) \quad \text{as} \quad R/a \to 0.$$

Hocking (1977) also anticipates a solution in terms of $\{\boldsymbol{\rho}\}$ but does not make use of the dual $\{\boldsymbol{\sigma}\}$ to evaluate his complex coefficients $\{C(s_n)\}$. Instead, he makes the residue of truncated sums for the stream function and radial velocity discontinuity at $z = 0$

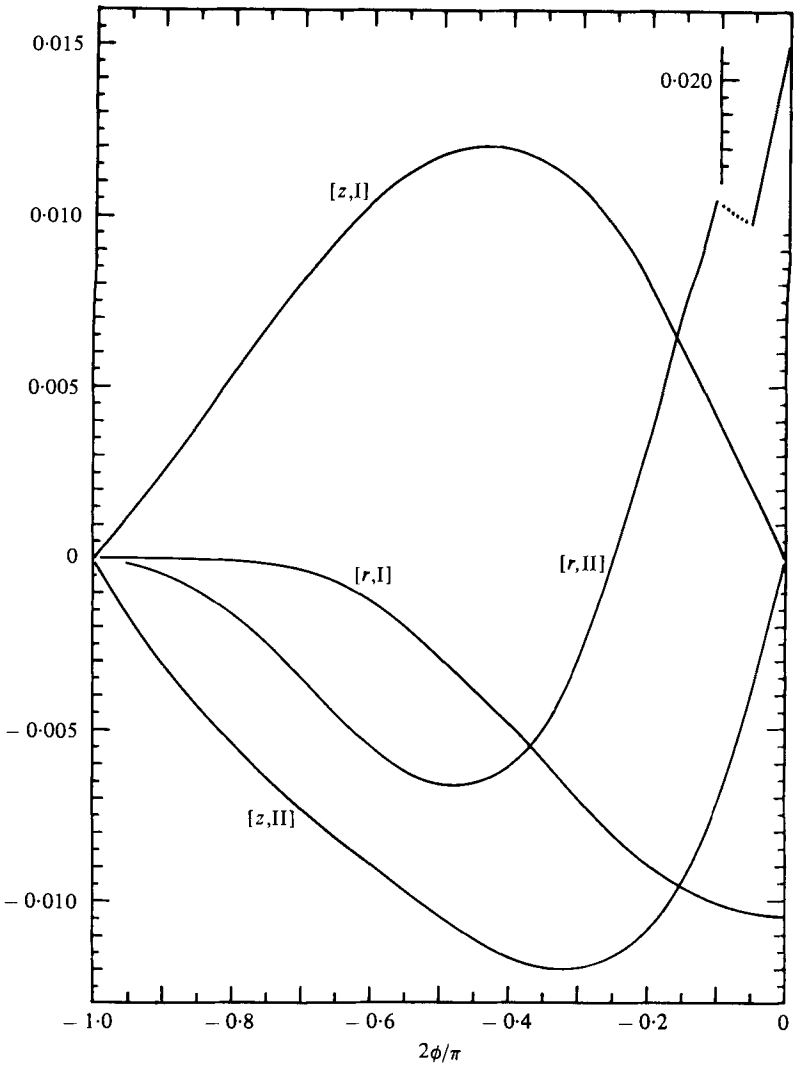


FIGURE 7. The difference between the outer and the anticipated asymptotic expression in the limit as $r \to 1$ and $z \to 0$, $\Delta \mathbf{v}^R$, can be evaluated at a distance $R = 0{\cdot}05a$ from the contact line for both components of the velocity vector using $\{[a, b]: a = r, z; b = \text{I, II}\}$,

where $$\Delta \mathbf{v}^R = \left([r, \text{I}] + \frac{\mu_A}{\mu_A + \mu_R}[r, \text{II}]\right)\hat{\mathbf{r}} + \left([z, \text{I}] + \frac{\mu_A}{\mu_A + \mu_R}[z, \text{II}]\right)\hat{\mathbf{z}}.$$

orthogonal to a set of cylinder functions all zero at $r = 1$. His sole published result, an asymptotic form for the integrated tangential stress on the solid wall, is in substantial agreement with our findings. However, a more thorough presentation of his results would have been useful.

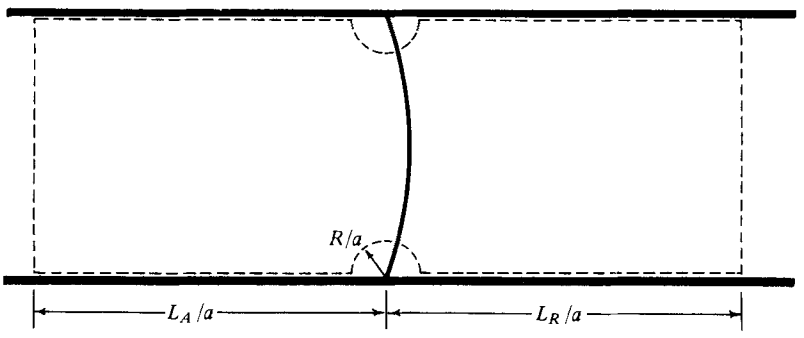


FIGURE 8. The slope of the meniscus within the intermediate region is calculated by balancing the forces acting on the fluid body enclosed by ———.

## 5. The pressure field and interface shape

The experimentally measurable quantities are: the pressure drop across a fixed length of capillary necessary to create a given volumetric flow rate, and, assuming the capillary is transparent, the shape of the fluid–fluid interface. These quantities are related through the integral form of the equation of conservation of linear momentum.

The difference in pressure between any two points on either side of the fluid–fluid interface can be calculated by using (3.1) along with the solution for the velocity field presented in §4. If the points are located more than two diameters from the interface, then

$$p^A_{Ca}(r, -L_A) - p^R_{Ca}(r, L_R) \doteq 8(\bar{\mu}_A L_A + \bar{\mu}_R L_R) - 1{\cdot}96^5(\bar{\mu}_A + \bar{\mu}_R) - 15{\cdot}27^8 \frac{\bar{\mu}_A \bar{\mu}_R}{\bar{\mu}_A + \bar{\mu}_R} + \Delta p_{Ca},$$

where $\Delta p_{Ca}$ denotes the pressure drop across the interface along the axis of the capillary, $p^A_{Ca}(0,0) - p^R_{Ca}(0,0)$. The constant term $-1{\cdot}96^5$ is due to that part of the solution given by $\psi_{\mathrm{I}}$; hence, it was evaluated by performing a double integral numerically. The second constant, $-15{\cdot}27^8$, coming from $\psi_{\mathrm{II}}$ was evaluated by extrapolating to $z = 0$ a series representation whose convergence is very slow at the point $(0,0)$. These coefficients represent deviations from the parallel flow pressure field in the vicinity of the interface.

The constant $\Delta p_{Ca}$ can be calculated by balancing the forces exerted on the body of fluid contained between the planes given by $z = -L_A/a$ and $z = L_R/a$, excluding the fluid within a fixed distance $R$ of the moving contact line; see figure 8. It is assumed that $R$ lies somewhere within the intermediate region. The force balance to within $O(R)$ as $R \to 0$ becomes

$$\left\{8\pi\left(\bar{\mu}_A \frac{L_A}{a} + \bar{\mu}_R \frac{L_R}{a}\right) - \pi(\bar{\mu}_A + \bar{\mu}_R)\left(\frac{8}{\pi}\ln\frac{R}{a} + 4{\cdot}62^4\right) - \frac{\pi\bar{\mu}_A\bar{\mu}_R}{\bar{\mu}_A + \bar{\mu}_R}\left(\frac{128}{\pi(\pi^2-4)}\ln\frac{R}{a} + 6{\cdot}57^6\right)\right\}$$
$$+\left\{-8(\bar{\mu}_A + \bar{\mu}_R) - \frac{128\,\bar{\mu}_A\bar{\mu}_R}{(\pi^2-4)(\bar{\mu}_A + \bar{\mu}_R)} - 2\pi\left.\frac{dh_{Ca}}{dr}\right|_{r=1-R/a}\right\}$$
$$-\pi\left\{p^A_{Ca}\left(-\frac{L_A}{a}\right) - p^R_{Ca}\left(\frac{L_R}{a}\right)\right\} \doteq 0.$$

The first bracket gives the force exerted on the body of fluid by the walls of the capillary, where the constants were determined by extrapolation procedures similar to

those of Hocking. The second bracket expresses the surface and viscous forces exerted on the body by the excluded fluid within the arc $R$, evaluated from an expression correct to $O(1)$. The final bracket gives the force exerted upon the ends of the body. The above equation can be interpreted as a representation of the shape of the interface within the intermediate region

$$\left.\frac{dh_{Ca}}{dr}\right|_{r=1-R/a} \doteq -\tfrac{1}{2}\Delta p_{Ca} - (\bar{\mu}_A+\bar{\mu}_R)\left(\frac{4}{\pi}\ln\frac{R}{a}+2{\cdot}60^3\right) + \frac{\bar{\mu}_A\bar{\mu}_R}{\bar{\mu}_A+\bar{\mu}_R}\left(\frac{-64}{\pi(\pi^2-4)}\ln\frac{R}{a}+0{\cdot}88^0\right). \tag{5.1}$$

This can be used to evaluate the boundary condition $(dh_{Ca}/dr)|_{r=1-R_I/a} = 0$. This condition determines $\Delta p_{Ca}$:

$$\Delta p_{Ca} = -(\bar{\mu}_A+\bar{\mu}_R)\left(\frac{8}{\pi}\ln\frac{R_I}{a}+5{\cdot}20^6\right)+\frac{\bar{\mu}_A\bar{\mu}_R}{\bar{\mu}_A+\bar{\mu}_R}\left(\frac{-128}{\pi(\pi^2-4)}\ln\frac{R_I}{a}+1{\cdot}76^0\right).$$

While balancing the forces exerted on the above material body of fluid has provided a convenient method for calculating the tangent to the interface shape in the intermediate region; in order to determine $dh_{Ca}/dr$ elsewhere, the normal stress balance at $z = 0$ must be integrated. The part due to $\psi_I$ is obtained by inverting numerically the appropriate sine-transform; the part due to $\psi_{II}$ is calculated both by extrapolating the integrated normal stress eigenfunction series to $z = 0$, and by the direct evaluation of the Green's function formulation at $z = 0$. Fitting polynomials with the desired asymptotic form to these two components, we have

$$\frac{dk_{Ca}}{dr} \doteq \{\bar{\mu}_A+\bar{\mu}_R\}\left\{\frac{4}{\pi}\left(r\ln\frac{2R_I}{a}-\frac{1}{r}\ln(1-r^2)\right)+(1-r^2)(-1{\cdot}583r-0{\cdot}475r^3 + 0{\cdot}447r^5-0{\cdot}852r^7)\right\}+\frac{\bar{\mu}_A\bar{\mu}_R}{\bar{\mu}_A+\bar{\mu}_R}\left\{\frac{64}{\pi(\pi^2-4)}\left(r\ln\frac{2R_I}{a}-\frac{1}{r}\ln(1-r^2)\right) + (1-r^2)(1{\cdot}409r-0{\cdot}076r^3+2{\cdot}078r^5-2{\cdot}287r^7)\right\}. \tag{5.2}$$

The maximum error in the expression multiplying $\bar{\mu}_A+\bar{\mu}_R$ is 0·002 based on evaluation at $r = (0{\cdot}05, 0{\cdot}10, \ldots, 0{\cdot}95)$; for the $\bar{\mu}_A\bar{\mu}_R/(\bar{\mu}_A+\bar{\mu}_R)$ part, the maximum difference from the Green's function results at the same points is 0·012.

Of course, the pressure drop and local shape of the interface given above represent only the lowest-order mode in $C_a$. The complete expressions must include the other small parameter terms:

$$p^A(r_1, -L_A/a) - p^R(r_2, +L_R/a) \sim 2(\theta_I-\tfrac{1}{2}\pi)+C_a[p^A_{Ca}(r_1,-L_A/a)-p^R_{Ca}(r_2,L_R/a)], \tag{5.3}$$

$$\frac{dh}{dr} \sim r(\tfrac{1}{2}\pi-\theta_I)+C_a\frac{dh_{Ca}}{dr}. \tag{5.4}$$

## 6. Dynamic contact angles

Besides the actual contact angle, $\theta$, four other contact angles have been introduced: $\theta_w$, defined by (1.1); $\theta_M$, defined by (1.2); $\theta_{\mathrm{H\&M}}$, the angle introduced by Huh & Mason, defined by the relationship $\cos\theta_{\mathrm{H\&M}} \equiv -a\mathscr{K}$, where $\mathscr{K}$ is the mean curvature of the fluid–fluid interface evaluated at its apex; and $\theta_{\mathrm{I}}$, the angle of inclination of the fluid–fluid interface at a distance $R_{\mathrm{I}}$ from the contact line (refer to §2). We are now in a position, in the light of the results of §5, to examine their dynamic behaviour and to calculate their interdependence.

In a static system all of the abovementioned angles are the same: however, when the contact line is in motion we find

$$\theta_w \sim \theta_{\mathrm{I}} - \frac{U}{\gamma}\left\{(\mu_A+\mu_R)\left(\frac{4}{\pi}\ln\frac{R_{\mathrm{I}}}{a}+3{\cdot}58\right)+\frac{\mu_A\mu_R}{\mu_A+\mu_R}\left(\frac{64}{\pi(\pi^2-4)}\ln\frac{R_{\mathrm{I}}}{a}+6{\cdot}76\right)\right\} \tag{6.1}$$

upon combining (1.1) and (5.3);

$$\theta_M \sim \theta_{\mathrm{I}} - \frac{U}{\gamma}\left\{(\mu_A+\mu_R)\left(\frac{4}{\pi}\ln\frac{R_{\mathrm{I}}}{a}+2{\cdot}10\right)+\frac{\mu_A\mu_R}{\mu_A+\mu_R}\left(\frac{64}{\pi(\pi^2-4)}\ln\frac{R_{\mathrm{I}}}{a}+8{\cdot}87\right)\right\} \tag{6.2}$$

upon combining (1.2) and (5.4); and

$$\theta_{\mathrm{H\&M}} \sim \theta_{\mathrm{I}} - \frac{U}{\gamma}\left\{(\mu_A+\mu_R)\left(\frac{4}{\pi}\ln\frac{R_{\mathrm{I}}}{a}+0{\cdot}573\right)+\frac{\mu_A\mu_R}{\mu_A+\mu_R}\left(\frac{64}{\pi(\pi^2-4)}\ln\frac{R_{\mathrm{I}}}{a}+7{\cdot}286\right)\right\} \tag{6.3}$$

upon combining the above-stated definition of $\theta_{\mathrm{H\&M}}$ with (5.2). For completeness, we present a relationship between $\theta_{\mathrm{I}}$ and $\theta$ based upon a solution of the motion of the fluids in the inner region in which a particular slip boundary condition is assumed:

$$\theta_{\mathrm{I}} \sim \theta + \frac{U}{\gamma}\left\{\frac{4}{\pi}(\mu_A+\mu_R)\left(1-\frac{\mu_A}{\mu_A+\mu_R}\ln\frac{L_{sR}}{L_{sA}}+\ln\frac{R_{\mathrm{I}}}{L_{sA}}\right)+\frac{\mu_A\mu_R}{\mu_A+\mu_R}\frac{64}{\pi(\pi^2-4)}\left(1+\ln\frac{R_{\mathrm{I}}}{\sqrt{(L_{sA}L_{sR})}}\right)\right\}; \tag{6.4}$$

refer to appendix B for details. The angles in the above expressions are in radians, and the trigonometric functions have been linearized about $\frac{1}{2}\pi$.

It is interesting to note that the dynamic behaviour of all three apparent contact angles – $\theta_w$, $\theta_M$ and $\theta_{\mathrm{H\&M}}$ – is influenced to some extent by the geometry of the outer region as evidenced by the appearance of the parameter $a$ in the bracketed expressions on the right-hand side of (6.1), (6.2) and (6.3). Consequently, these angles do not represent material properties of the system. This is not surprising when one recognizes that each of these angles is calculated from a quantity which depends on the dynamics of the fluids in the *outer* region: $\theta_w$ is calculated from the pressure drop down the capillary; $\theta_M$ is calculated from $H$; and $\theta_{\mathrm{H\&M}}$ is calculated from the mean curvature of the meniscus at its apex. The dependence on geometry becomes explicit when any one

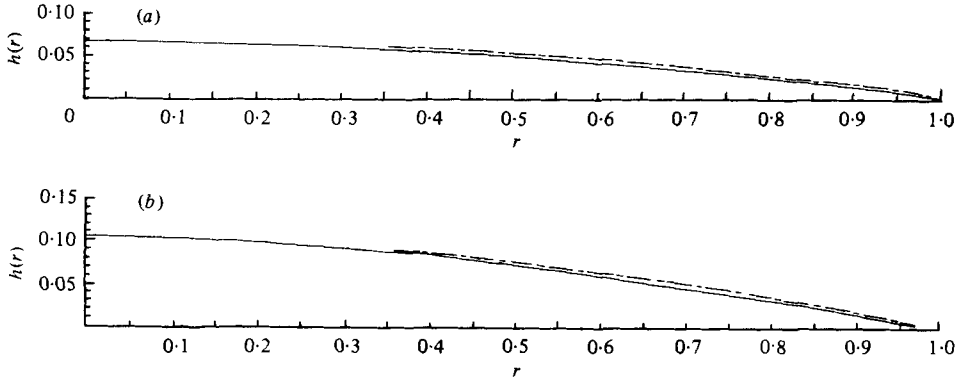


FIGURE 9. The solid curve in (*a*) and (*b*) is the solution for the meniscus when $\mu_R \ll \mu_A$, and $\mu_R = \mu_A$, respectively. In both cases it is assumed $U(\mu_A+\mu_R)/\gamma = 0{\cdot}02$ and $\theta_I = 90°$ at $R_I/a = 0{\cdot}001$. The dashed curve is a segment of a circle passing through the apex, $h(0)$, and the contact line.

of these apparent contact angles is evaluated for two systems identical in every way except that the radius of the capillaries is different, for example,

$$\theta_M(a_1)-\theta_M(a_2) \sim \frac{U}{\gamma}\left\{(\mu_A+\mu_R)\frac{4}{\pi}\ln\frac{a_1}{a_2}+\frac{\mu_A\mu_R}{\mu_A+\mu_R}\frac{64}{\pi(\pi^2-4)}\ln\frac{a_1}{a_2}\right\}.$$

This difference is due entirely to the independence of the size of the inner region on the value of $a$. Note that no parameter which depends on the model of the inner region appears in the above expression.

The entire effect of the fluid motion in the inner region on the experimentally measurable quantities $\theta_w$, $\theta_M$ and $\theta_{H\&M}$† appears in the dynamic behaviour of the intermediate angle, $\theta_I$. Two factors contribute to $\theta_I$, as illustrated by (6.4): (i) the dynamic behaviour of the actual contact angle, $\theta$, and (ii) the bending of the meniscus in the inner region due to hydrodynamic forces. The latter directly depends on the mechanism used to remove the singularity at the contact line. It is evident from (6.1), (6.2) and (6.3) that measurements of the pressure drop and $H$ can, at most, be used to determine the dynamic behaviour of $\theta_I$: *they cannot be used to deduce anything about the nature of the fluids in the inner region or the dynamic behaviour of* $\theta$.

That the various contact angles can take on different values is illustrated by the following example. Consider a capillary of radius $a = 0{\cdot}05$ cm through which fluids are moving at a speed of $U(\mu_A+\mu_R)/\gamma = 0{\cdot}02$ with an intermediate angle $\theta_I = 90°$ at a distance $R_I = 0{\cdot}5\times10^{-6}$ m from the contact line (this choice of parameters is consistent with Hoffman's correlation). Two cases are calculated, that of $\mu_R = 0$ and $\mu_A = \mu_R$. The solid lines in figure 9(*a*, *b*) represent the solution of the shape of the interface. The dashed lines represent segments of spheres which pass through the apex of the meniscus and the contact line. Even for this low value of the capillary number the meniscus deviates somewhat from a spherical segment. The angle formed between the dashed line and the wall, $\theta_M$, is 98° (102°)‡, while that determined by the pressure drop

† To our knowledge, experimentally measured values of $\theta_{H\&M}$ have yet to be reported.

‡ These correspond to $\mu_R = 0$ and $\mu_R = \mu_A$, respectively.

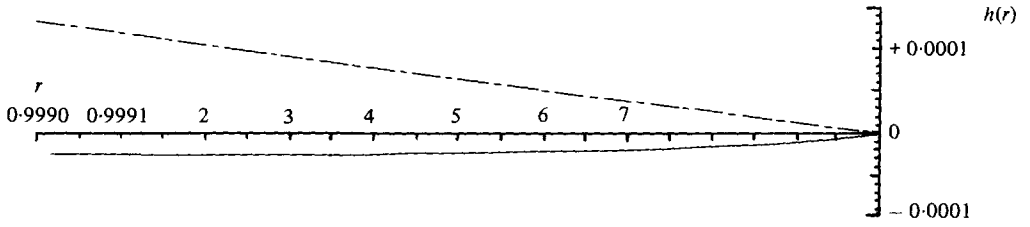


FIGURE 10. The shape of the meniscus in figure 9(*a*) very close to the contact line assuming $L_{sA} = 0{\cdot}5 \times 10^{-6}$ cm.

down the capillary, $\theta_w$, is 96° (101°).† Nevertheless, if a tangent to the interface is drawn close to the contact line on figure 9, following the procedure of Rose & Heins (1962), the angle measured with a protractor is approximately 94° (96°). This is smaller than the apparent contact angles, but larger than the intermediate angle, $\theta_{\mathrm{I}}$. For the sake of demonstration, if we use the inner solution presented in appendix B with $L_{sA} = L_{sR} = 5 \times 10^{-9}$ m then the shape of the meniscus close to the wall is given in figure 10. The actual contact angle, given by (6.4), is 82° (76°), which differs quite a bit from the angle formed by the dashed line.

## 7. Discussions and conclusions

An appropriate value for $R_{\mathrm{I}}$ has yet to be established. The only property which it must have (refer to §2) is that it lie 'well within' the intermediate region, i.e. the region where both inner and outer solutions are valid. However, the size of this region and the degree to which both solutions coincide depends on the value of $L_i/L_\phi$. If it is assumed that flow through a capillary with the inner region modelled as in appendix B typifies flow in any geometry with any model of the inner region, and that $L_i \lesssim 10^{-8}$ m and $L_\phi \gtrsim 10^{-5}$ m, then a good choice is $R_{\mathrm{I}} = 0{\cdot}5 \times 10^{-6}$ m. This is illustrated by comparing the values of the slope of the interface as predicted by the inner and outer solutions for the example cited at the end of §6; refer to table 3. The two solutions differ by less than $\pm 0{\cdot}5°$ for $5 \times 10^{-9}$ m $< R < 5 \times 10^{-6}$ m (note that the minimum in the meniscus at $R \approx 5 \times 10^{-9}$ m (refer to figure 10) occurs in *both* solutions). It should be remembered that dynamic apparent contact angle measurements cannot be reproduced to better than $\pm 1°$ and 2°.

It can easily be seen how the displacement of immiscible fluids through a capillary can be used as a device for obtaining basic modelling information that is necessary for solving boundary-value problems involving the moving contact line. For a given material system, two immiscible fluids and a solid, the dependence of $H$ on the speed of the contact line can be measured. This is sufficient, together with a detailed fluid-mechanical analysis of the outer region, to calculate the dynamic behaviour of $\theta_{\mathrm{I}}$.

For the case in which $H/a \ll 1$, $\theta_{\mathrm{I}}(U)$ is obtained by substituting the experimentally determined $H(U)$ into the expression:

$$\theta_{\mathrm{I}} \sim \frac{2H}{a} + \frac{\pi}{2} + \frac{U}{\gamma}\left\{(\mu_A + \mu_R)\left(\frac{4}{\pi}\ln\frac{R_{\mathrm{I}}}{a} + 2{\cdot}10\right) + \frac{\mu_A \mu_R}{\mu_A + \mu_R}\left(\frac{64}{\pi(\pi^2 - 4)}\ln\frac{R_{\mathrm{I}}}{a} + 8{\cdot}87\right)\right\}.$$

† It is interesting to note that $\theta_w$ and $\theta_M$ can have similar values even though they both differ from $\theta$. Hence, Blake's reported experimental agreement between these two angles does not imply that he is measuring the dynamic behaviour of the actual contact angle.

| $R/L_s$ | $r$ | $90° + \arctan\left(a\frac{dh_{\text{inner}}}{dR}\right)^{\dagger}$ | $\arctan\left(-\frac{dh_{\text{outer}}}{dr}\right)^{\ddagger} - \arctan\left(a\frac{dh_{\text{inner}}}{dR}\right)$ |
|---|---|---|---|
| 0·02 | 0·9999998 | 81·96° | −4·19° |
| 0·20 | 0·999998 | 82·49° | −1·49° |
| 1·0 | 0·99999 | 83·72° | −0·41° |
| 2·0 | 0·99998 | 84·50° | −0·19° |
| 10·0 | 0·99990 | 86·66° | −0·02° |
| 20·0 | 0·99980 | 87·66° | −0·01° |
| 100·0 | 0·999 | 90·00° | −0·00° |
| 200·0 | 0·998 | 91·01° | −0·02° |
| $10^3$ | 0·99 | 93·35° | −0·10° |
| $2·0 \times 10^3$ | 0·98 | 94·36° | −0·18° |
| $10^4$ | 0·9 | 96·68° | −0·82° |
| $2·0 \times 10^4$ | 0·8 | 97·68° | −1·68° |
| $4·0 \times 10^4$ | 0·6 | 98·67° | −5·05° |

† Calculated from (B 3).
‡ Calculated from (5.4).

TABLE 3. The slope of the interface in the intermediate region for $C_a = 0·02$, $\mu_R = 0$, $a = 500\,\mu$m, $L_s = 5 \times 10^{-3}\,\mu$m, $R_I = 0·5\,\mu$m, $\theta_I = 90°$.

The implicit dependence of $H(U)$ on $a$ cancels the explicit dependence of the bracketed expression on $a$. In order to predict the spreading of the same liquid on the same solid, however, in a different geometry, for example a drop of liquid ($\mu_A$) spreading over a planar surface initially covered with fluid ($\mu_R$), one need only solve for the dynamics of the fluid in the outer region. The boundary condition that $\theta = \theta_I(U)$ at a distance $R_I$ from the contact line is sufficient for determining the shape of the meniscus in the outer region to $O(C_a)$; no *ad hoc* assumption need be made about the deformation of the meniscus in the inner region (a case in point is Greenspan, 1978).

On the other hand, knowledge of the dynamic behaviour of $\theta_I$ does not represent sufficient information for the physical chemist who is interested in identifying the mechanism by which liquids spread on solids. Although it can be used to establish the inadequacy of a given model of the inner region for a particular material system, it does not contain sufficient information to identify either the dynamic behaviour of the actual contact angle or the mechanism by which the singularity at the moving contact line is removed.

Until experimental techniques are discovered which can probe the inner region, parameterizing the outer region in terms of the empirically measurable quantity $\theta_I$ appears to be an adequate approach for fluid-mechanicians interested in analysing flow fields with moving contact lines.

The authors are grateful for the support received from the National Science Foundation under grants ENG75-10297 and ENG77-10167.

## Appendix A

An integral expression for $\psi_{II}$ can be obtained by taking its sine-transformation in the $z$ co-ordinate

$$\overline{\psi}_{II}(r;s) \equiv \int_0^\infty \psi_{II}(r,z)\sin(sz)\,dz$$

and

$$\psi_{II}(r,z) = \frac{2}{\pi}\int_0^\infty \overline{\psi}_{II}(r;s)\sin(sz)\,ds$$

valid for $0 < z < \infty$ and $0 < r < 1$. The transformed Stokes–Beltrami equation and boundary conditions are

$$\left[r\frac{d}{dr}\frac{1}{r}\frac{d}{dr} - s^2\right]^2 \overline{\psi}_{II} = s^3\psi_{II}(r,0) - 2s^2\left(r\frac{\partial}{\partial r}\frac{1}{r}\frac{\partial\psi_{II}}{\partial r}\right)\Big|_{z=0} - s\frac{\partial^2\psi_{II}}{\partial z^2}\Big|_{z=0}$$

and

$$\overline{\psi}_{II} = 0, \quad \frac{1}{r}\frac{d\overline{\psi}_{II}}{dr} = 0 \quad \text{at} \quad r = 1.$$

At the plane $z = 0$ the boundary conditions are

$$\psi_{II} = 0, \quad \frac{1}{r}\frac{\partial^2\psi_{II}}{\partial z^2} = \tau(r).$$

It follows directly that

$$\overline{\psi}_{II} = -\frac{r}{2}\left\{\int_0^r G(\rho,r;s)\rho\tau(\rho)\,d\rho + \int_r^1 G(r,\rho;s)\rho\tau(\rho)\,d\rho\right\}$$

where

$$\begin{aligned}
G(\rho,r;s) = {} & \{I_1(\rho s)[2I_0(s)+sI_1(s)][rI_1(s)K_0(rs)-I_1(rs)K_0(s)] \\
& +\rho I_2(\rho s)[2I_0(s)+sI_1(s)][I_1(rs)K_1(s)-I_1(s)K_1(rs)] \\
& +\rho s I_2(\rho s)I_0(s)[I_0(s)K_1(rs)-rI_0(rs)K_1(s)] \\
& +sI_1(\rho s)I_0(s)[rI_0(rs)K_0(s)-rI_0(s)K_0(rs)] \\
& +[\rho s I_0(\rho s)K_0(s)-sI_1(\rho s)K_1(s)][I_0(s)I_1(rs)-rI_0(rs)I_1(s)]\} \\
& \times\{2I_0(s)I_1(s)-sI_0(s)^2+sI_1(s)^2\}^{-1}.
\end{aligned}$$

The modified Bessel functions $K_0$ and $K_1$ used in the above expression are discussed by Abramowitz & Stegun (1964).

## Appendix B

We shall, for illustrative purposes, calculate the inner solution assuming that the axial velocity (from the moving reference frame) is given by

$$w^K = -\frac{|z|}{|z| + L_{sK}/a} \quad \text{at} \quad r = 1 \quad \text{for} \quad K = A, R,$$

where the parameters $L_{sA}$ and $L_{sR}$ are slip lengths in the advancing and receding fluids, respectively. This model was used by Dussan V. (1976) for a single liquid. Given such a model with its associated inner length scale $L_{s_m}$ ($L_{s_m} \equiv \max_{K=A,R} L_{sK}$ in this case), the appropriate inner problem can be generated by rescaling the independent variables $z$

and $R$ reduced to Stokes flow in two dimensions, provided that $L_{s_m}/a$ is very small (Huh & Mason 1977).

Expanding as before in small parameters and using the polar co-ordinate system introduced in figure 2, the two-dimensional form of the inner interface shape is expressed as

$$h(R/a) \sim (\theta(U) - \tfrac{1}{2}\pi)\, R/a + C_a h_{C_a}^{\text{inner}}(R/a),$$

where $h_{C_a}^{\text{inner}}$ is determined by the zero-order inner velocity field satisfying

$$\left[\frac{1}{R}\frac{\partial}{\partial R} R \frac{\partial}{\partial R} + \frac{1}{R^2}\frac{\partial^2}{\partial \phi^2}\right]^2 \Phi^K = 0;$$

$$\Phi^K = 0, \quad \frac{\partial \Phi^K}{\partial \phi} = \frac{(-1)^K (R/a)^2}{R/a + L_{sK}/a} \quad \text{on} \quad \phi = \tfrac{1}{2}(-1)^K \pi;$$

$$\phi^K = 0, \quad \left[\frac{\partial \Phi}{\partial \phi}\right] = 0, \quad \text{and} \quad \left[\bar{\mu}\frac{\partial^2 \Phi}{\partial \phi^2}\right] = 0 \quad \text{on} \quad \phi = 0$$

and

$$\frac{dh_{C_a}^{\text{inner}}}{dR} = 0 \quad \text{at} \quad R = 0,$$

where $(-1)^A \equiv -1$ and $(-1)^R \equiv +1$.

A solution for $\Phi^K$ is obtained in a straightforward manner using the Mellin transformation. We find the transformed steam function

$$\begin{aligned}\tilde{\Phi}^K = {} & \frac{\pi}{2}\left(\frac{L_{sK}}{a}\right)^{s+1} \frac{\operatorname{cosec} \pi s}{\cos \frac{1}{2}\pi s} \left[\sin(s|\phi|) + \sin(s+2)|\phi|\right] \\ & - \frac{\tilde{\tau}(s)}{4(s+1)\bar{\mu}_K} \left[\{(s+1)\tan \tfrac{1}{2}\pi s + (s+2)\cot \tfrac{1}{2}\pi s\} \sin(s|\phi|) - \cos(s|\phi|)\right. \\ & \left. + \{(s+1)\tan \tfrac{1}{2}s\pi + s \cot \tfrac{1}{2}s\pi\} \sin(s+2)|\phi| + \cos(s+2)|\phi|\right],\end{aligned}$$

where $\tilde{\tau}$, which represents the transformed tangential stress on $\phi = 0$, is given exactly by

$$\tilde{\tau}(s) = \frac{\bar{\mu}_A \bar{\mu}_R}{\bar{\mu}_A + \bar{\mu}_R}\left[\frac{2\pi(s+1)^2([L_{sA}/a]^{s+1} + [L_{sR}/a]^{s+1}) \operatorname{cosec}(\pi s) \sec \frac{1}{2}\pi s}{(s+1)^2 \tan \frac{1}{2}s\pi + s(s+2)\cot \frac{1}{2}s\pi}\right].$$

To obtain $\phi^K$ the inverse transform is used:

$$\phi^K = \frac{1}{2\pi i}\int_{\sigma_0 - i\infty}^{\sigma_0 + i\infty} \tilde{\Phi}(s;\phi)\left(\frac{R}{a}\right)^{-s} ds \quad \text{for} \quad -2 < \sigma_0 < -1.$$

The radius of curvature of the interface within the inner region is equal to the sum of the pressure and normal viscous stress differences across $\phi = 0$. This is integrated exactly to give

$$a\frac{dh_{C_a}^{\text{inner}}}{dR} = -\frac{R}{a}[\![p_{C_a}]\!] - a^2 \int_0^{R/a} \left[\!\!\left[\bar{\mu}\left\{\left(R\frac{\partial}{\partial R}\frac{1}{R}\frac{\partial}{\partial R} + \frac{2}{R^2}\right)\frac{\partial \Phi}{\partial \phi} + \frac{1}{R^2}\frac{\partial^3 \Phi}{\partial \phi^3}\right\}\right]\!\!\right] dR/a, \quad \text{(B 1)}$$

where $h$, as before, represents the $z$ location of the interface, though now as a function of $R/a$, on $\phi = 0$.

Since our objective is to derive a relationship between $\theta(U)$ and $\theta_{\text{I}}$, all we need evaluate is $dh_{C_a}^{\text{inner}}/dR$ in the limit as $R/L_s \to \infty$ because

$$\theta_{\text{I}} - \tfrac{1}{2}\pi = a\frac{dh}{dR}\bigg|_{R/a = R_{\text{I}}/a} \sim \theta(U) - \tfrac{1}{2}\pi + C_a a \frac{dh_{C_a}^{\text{inner}}}{dR}\bigg|_{R/a = R_{\text{I}}/a}, \quad \text{(B 2)}$$

where $R_{\mathrm{I}}$ lies somewhere within the intermediate region.

Restating equation (B 1) in terms of the solution for $\Phi^K$ gives

$$a\frac{dh_{C_a}^{\text{inner}}}{dR} = -\frac{R}{a}[\![p_{C_a}]\!]^{\text{inner}} + \bar{\mu}_A g(R/L_{sA}) + \bar{\mu}_R g(R/L_{sR}) + \frac{1}{2}\frac{\bar{\mu}_A\bar{\mu}_R}{\bar{\mu}_A+\bar{\mu}_R}\{f(R/L_{sA})+f(R/L_{sR})\}$$

where

$$g(x) \equiv +i\int_{\sigma_0-i\infty}^{\sigma_0+i\infty}[\operatorname{cosec}(\pi s)\sec\tfrac{1}{2}\pi s]\,x^{-(s+1)}\,ds;$$

and

$$f(x) \equiv -4i\int_{\sigma_0-i\infty}^{\sigma_0+i\infty}\frac{x^{-(s+1)}(s+1)^2\operatorname{cosec}(\pi s)\sec\tfrac{1}{2}\pi s}{(s+1)^2+s(s+2)\cot^2\tfrac{1}{2}\pi s}\,ds$$

for $-2 < \sigma_0 < -1$.

The function $g$ has been evaluated in closed form by Dussan V. (1976):

$$g(R/L_s) \sim \frac{4}{\pi}\ln\frac{R}{L_s} + O\left(\frac{L_s^2}{R^2}\ln\frac{R}{L_s}\right) \quad \text{as} \quad R/L_s \to \infty.$$

Upon numerical evaluation of the function $f$ we found that

$$f(R/L_s) \sim \frac{64}{\pi(\pi^2-4)}\ln\frac{R}{L_s} + O\left(\frac{L_s^2}{R^2}\ln\frac{R}{L_s}\right) \quad \text{as} \quad R/L_s \to \infty.$$

It is also possible to show that

$$\frac{R}{a}[\![p_{C_a}]\!]^{\text{inner}} \sim -\frac{4}{\pi}(\bar{\mu}_A+\bar{\mu}_R) - \frac{64}{\pi(\pi^2-4)}\frac{\bar{\mu}_A\bar{\mu}_R}{(\bar{\mu}_A+\bar{\mu}_R)} + O\left(\frac{L_s^2}{R^2}\ln\frac{R}{L_s}\right) \quad \text{as} \quad R/L_s \to \infty.$$

Upon substituting the above expressions into equation (B2) we get

$$\theta_{\mathrm{I}} \sim \theta(U) + C_a\left\{\frac{4}{\pi}(\bar{\mu}_A+\bar{\mu}_R)\left(1 - \frac{\bar{\mu}_R}{\bar{\mu}_A+\bar{\mu}_R}\ln\frac{L_{sR}}{L_{sA}} + \ln\frac{R_{\mathrm{I}}}{L_{sA}}\right) + \frac{\bar{\mu}_A\bar{\mu}_R}{\bar{\mu}_A+\bar{\mu}_R}\frac{64}{\pi(\pi^2-4)}\left(1+\ln\frac{R_{\mathrm{I}}}{(L_{sA}L_{sR})^{\frac{1}{2}}}\right)\right\}.$$

For the case of $\bar{\mu}_R \equiv 0$, the slope, $dh_{C_a}^{\text{inner}}/dR$, has been solved exactly (Dussan V. 1976) giving

$$a\frac{dh}{dR} \sim \theta(U) - \frac{\pi}{2} + C_a\left\{\frac{4R/L_{sA}}{1+(R/L_{sA})^2} - \frac{4(R/L_{sA})^3}{([1+(R/L_{sA})^2]^2} + \frac{12(R/L_{sA})^2\ln(R/L_{sA}) + 4(R/L_{sA})^2}{\pi[1+(R/L_{sA})^2]} - \frac{8(R/L_{sA})^4\ln(R/L_s)}{\pi[1+(R/L_{sA})^2]^2}\right. \quad \text{(B 3)}$$

We make use of the above expressions in §§ 6 and 7.

## REFERENCES


Abramowitz, M. & Stegun, I. 1964 *Handbook of Mathematical Functions.* Washington: National Bureau of Standards.

Batchelor, G. K. 1970 *An Introduction to Fluid Dynamics.* Cambridge University Press.

Bhattacharji, S. & Savic, P. 1965 Real and apparent non-Newtonian behaviour in viscous pipe flow of suspensions driven by a fluid piston. *Proc. Heat Transfer Fluid Mech.*, p. 248.

BLAKE, T. D. 1968 Ph.D. thesis. *Department of Physical Chemistry, University of Bristol*. England.

BLAKE, T. D. & HAYNES, 1969 Kinetics of liquid/liquid displacement. *J. Colloid Interface Sci.* **3**, 421.

DUSSAN V., E. B. 1976 The moving contact line: the slip boundary condition. *J. Fluid Mech.* **77**, 665.

DUSSAN V., E. B. 1977 Immiscible liquid displacement in a capillary tube: the moving contact line. *A.I.Ch.E.J.* **23**, 131.

DUSSAN V., E. B. 1979 On the spreading of liquids on solid surfaces: static and dynamic contact lines. *Ann. Rev. Fluid Mech.* **11**, 371.

DUSSAN V., E. B. & DAVIS, S. H. 1974 On the motion of a fluid–fluid interface along a solid surface. *J. Fluid Mech.* **65**, 71.

ELLIOTT, G. E. P. & RIDDIFORD, A. C. 1967 Dynamic contact angles. I. The effect of impressed motion. *J. Colloid Interface Sci.* **23**, 389.

GREENSPAN, H. P. 1978 On the motion of a small viscous droplet that wets a surface. *J. Fluid Mech.* **84**, 125.

HANSEN, R. J. & TOONG, T. Y. 1971*a* Interface behavior as one fluid completely displaces another from a small-diameter tube. *J. Colloid Interface Sci.* **36**, 410.

HANSEN, R. J. & TOONG, T. Y. 1971*b* Dynamic contact angle and its relationship to forces of hydrodynamic origin. *J. Colloid Interface Sci.* **37**, 196.

HOCKING, L. M. 1976 A moving fluid interface on a rough surface. *J. Fluid Mech.* **76**, 801.

HOCKING, L. M. 1977 A moving fluid interface. Part 2. The removal of the force singularity by a slip flow. *J. Fluid Mech.* **79**, 209.

HOFFMAN, R. 1975 A study of the advancing interface I. Interface shape in liquid–gas systems. *J. Colloid Interface Sci.* **50**, 228.

HUH, C. & MASON, S. G. 1977 The steady movement of a liquid meniscus in a capillary tube. *J. Fluid Mech.* **81**, 401.

HUH, C. & SCRIVEN, L. E. 1971 Hydrodynamic model of steady movement of a solid/liquid/fluid contact line. *J. Colloid Interface Sci.* **35**, 85.

JIANG, T. S., OH, S. G. & SLATTERY, J. C. 1978 Correlation for dynamic contact angles. *J. Colloid Interface Sci.* In press.

ROSE, W. & HEINS, R. W. 1962 Moving interfaces and contact angle rate-dependence. *J. Colloid Interface Sci.* **17**, 39.

SMITH, R. C. T. 1952 The bending of a semi-infinite stip. *Australian J. Sci. Res.* A **5**, 227.

WAGNER, M. H. 1975 Developing flow in circular conduits: transition from plug flow to pipe flow. *J. Fluid Mech.* **72**, 257.

WASHBURN, E. W. 1921 The dynamics of capillary flow. *Physical Rev.* **17**, 243.

WEST, G. D. 1911–1912 On resistance to the motion of a thread of mercury in a glass tube. *Proc. Roy. Soc.* A **86**, 20.

YARNOLD, G. D. 1938 The motion of a mercury index in a capillary tube. *Proc. Phys. Soc. London* **50**, 540.

YOO, J. Y. & JOSEPH, D. D. 1978 Stokes flow in a trench between concentric cylinders. *SIAM J. Appl. Math.* **32**.